Fourier transform channeled spectropolarimetry in the MWIR

Michael W. Kudenov,[1] Nathan A. Hagen, [1] Eustace L. Dereniak, [1] and Grant R. Gerhart[2]

[1]College of Optical Science, The University of Arizona, 1630 E. University Blvd., Tucson, AZ 85721
[2]U.S. Army TACOM, 6501 E. 11 Miles Rd., Warren, MI 48397

Abstract: A complete Fourier Transform Spectropolarimeter in the MWIR is demonstrated. The channeled spectral technique, originally developed by K. Oka, is implemented with the use of two Yttrium Vanadate (YVO_4) crystal retarders. A basic mathematical model for the system is presented, showing that all the Stokes parameters are directly present in the interferogram. Theoretical results are compared with real data from the system, an improved model is provided to simulate the effects of absorption within the crystal, and a modified calibration technique is introduced to account for this absorption. Lastly, effects due to interferometer instabilities on the reconstructions, including nonuniform sampling and interferogram translations, are investigated and techniques are employed to mitigate them.

OCIS codes: (300.6340) Spectroscopy, infrared; (120.2130) Ellipsometry and polarimetry

References and links

1. P. Griffiths and J. D. Haseth, "Fourier Transform Infrared Spectrometry," (John Wiley & Sons, Inc., NY, 1986).
2. K. Oka and T. Kato, "Spectroscopic Polarimetry with a Channeled Spectrum," Opt. Lett. **24,** 1475-1477 (1999).
3. T. Kusunoki and K. Oka, "Fourier spectroscopic measurement of polarization using birefringent retarders," Jap. Soc. of Ap. Phys. **61**, 871 (2000).
4. M. Kudenov, N. Hagen, H. Luo, *et al*, "Polarization acquisition using a commercial Fourier transform spectrometer in the MWIR," in *Infrared Detectors and Focal Plane Arrays VII*, E. Dereniak and R. Sampson, eds., Proc. SPIE 688401 (2006).
5. A. Taniguchi, K. Oka, H. Okabe, and M. Hayakawa, "Stabilization of a channeled spectropolarimeter by self-calibration," Opt. Lett. **31,** 3279-3281 (2006).
6. J. Connes, "Aspen International Conference on Fourier Spectroscopy," G.A. Vanasse, A.T. Stair, Jr., and D.J. Baker, eds. (Air Force Cambridge Labs Report, No. 114), 83 (1970).
7. Dennis Goldstein, "Polarized Light" (Marcel Dekker, NY, 2003).
8. R. Bell, "Introductory Fourier Transform Spectroscopy," (Academic Press, 1972).
9. D. Naylor, T. Fulton, P. Davis, I. Chapman *et al*, "Data processing pipeline for a time-sampled imaging Fourier transform spectrometer," in *Imaging Spectrometry X*, S. Shen and P. Lewis, eds., Proc. SPIE 560096 (2004).
10. Vidi Saptari, "Fourier-transform spectroscopy instrumentation engineering," (SPIE Press, Bellingham, WA, 2004).
11. Q. H. Liu and N. Nguyen, "An accurate algorithm for nonuniform fast fourier transforms," IEE Mic. Guid. Wave Lett. **8,** 18-20 (1998).
12. A. Dutt and V. Rokhlin, "Fast fourier transforms for nonequispaced data," Siam J. Sci. Comput. **14,** 1368-1393 (1993).

1. Introduction

A Fourier Transform Spectrometer (FTS) has many advantages over other forms of spectroscopic measurement, such as a diffraction grating spectrometer, in the MWIR. Predominantly, the FTS maintains the throughput (Jacquinot) and multiplex (Fellgett) advantages [1]. Yet aside from this, the FTS has another unique benefit for working with the

#83298 - $15.00 USD Received 22 May 2007; revised 13 Sep 2007; accepted 14 Sep 2007; published 21 Sep 2007

channeled spectropolarimetric technique implemented by K. Oka, where the Stokes vector information is modulated onto the spectrum via several carrier frequencies [2]. These carrier frequencies can be observed as separate entities in the interferogram taken from an FTS, thereby providing a more direct means of acquiring the spectropolarimetric data [3].

First, we will describe the theoretical model behind the spectropolarimetric technique with an FTS. This will be followed with our laboratory results obtained by a commercial FTS in the MWIR using Yttrium Vanadate (YVO_4) crystal retarders. Detailed error analyses are provided, and an improved system model is discussed. Lastly, the improved model is used to provide an enhanced calibration technique to remove the effect of the dichroism in the YVO_4.

2. System model

The basic setup of the Fourier Transform Spectropolarimeter (FTSP) is shown in Fig. 1. It consists of two high-order retarders R_1 and R_2 with thicknesses d_1 and d_2 followed by an analyzer. The orientation of the retarder's fast axes relative to the transmission axis of the analyzer is 0° and 45° for R_1 and R_2, respectively. The output is then sent into an interferometer and the data recorded.

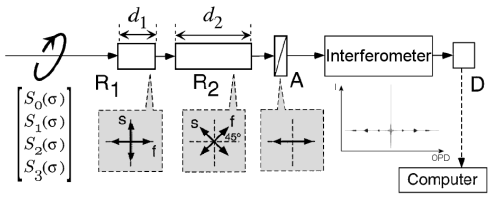

Fig. 1. Basic FTSP block diagram.

To create a theoretical model of the above system, we utilize plane-wave propagation in a typical Twyman-Green interferometer to observe the functional form of the interferogram $I(\sigma,z)$ [4]. Performing this analysis yields,

$$I(\sigma,z) \propto \frac{(1+\cos(\phi_z))}{2}\left[S_0 + S_1\cos(\phi_2) + S_2\sin(\phi_1)\sin(\phi_2) - S_3\cos(\phi_1)\sin(\phi_2)\right] \tag{1}$$

where S_0, S_1, S_2, and S_3 are the Stokes parameters related to the intensity, linear 0° or 90°, linear +45° or -45°, and right or left circular polarizations, respectively. The phase terms ϕ_1, ϕ_2, and ϕ_z are implicitly dependent upon wavenumber σ (λ^{-1}) and are defined as

$$\phi_1(\sigma) = 2\pi B(\sigma) d_1 \sigma \tag{2}$$

$$\phi_2(\sigma) = 2\pi B(\sigma) d_2 \sigma \tag{3}$$

$$\phi_z(\sigma) = 2\pi \Delta z \sigma \tag{4}$$

where Δz is the optical path difference (OPD) from the interferometer, $B(\sigma) = \left(n_e(\sigma) - n_o(\sigma)\right)$ is the birefringence of the crystal, and d_1, d_2 are the aforementioned retarder thicknesses. Expansion of Eq. 1 can be seen in Eq. 5. Here the constant offset has been suppressed since it's independent of Δz; it provides no viable spectral information in the Fourier transform.

$$\begin{aligned} I(\sigma,z) \propto\ & \frac{S_0}{2}\cos(\phi_z) + \frac{S_1}{4}\left(\cos(\phi_z+\phi_2) + \cos(\phi_z-\phi_2)\right) + \\ & \frac{S_2}{8}\left[\cos(\phi_z+\phi_1+\phi_2) + \cos(\phi_z-\phi_1-\phi_2) - \cos(\phi_z+\phi_1-\phi_2) - \cos(\phi_z-\phi_1+\phi_2)\right] + \\ & \frac{S_3}{8}\left[\sin(\phi_z+\phi_1+\phi_2) - \sin(\phi_z-\phi_1-\phi_2) - \sin(\phi_z+\phi_1-\phi_2) + \sin(\phi_z-\phi_1+\phi_2)\right] \end{aligned} \tag{5}$$

#83298 - $15.00 USD Received 22 May 2007; revised 13 Sep 2007; accepted 14 Sep 2007; published 21 Sep 2007

From Eq. 5, there are seven distinct channels which contain the data related to the input polarization parameters S_0, S_1, S_2, and S_3. These channels can be seen superimposed onto real data from the instrument in Fig. 2. It should be noted that the data in this figure is Eq. 5 integrated over σ from 2000 cm^{-1} to approximately 4100 cm^{-1}.

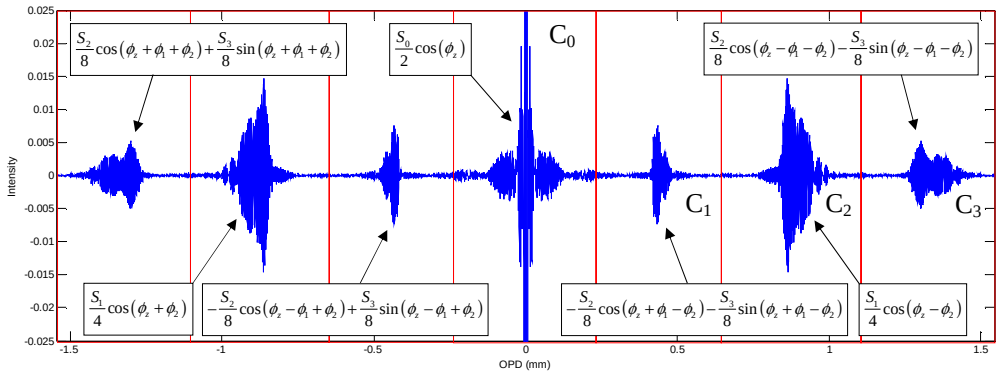

Fig. 2. The 7 channels in the interferogram are separated in OPD space by the retardances φ_1 and φ_2. Shown is a real channeled interferogram with the functional forms of each channel listed, along with the relative channel widths indicated by the boxes. Spacing between each channel is for a 2:1 thickness ratio (d_2:d_1) using our setup, which will be described in §4.

Demodulation of the spectral Stokes vectors can now be performed by filtering the desired channels, followed by a Fourier transformation. Performing this on channels C_0, C_2, and C_3 per Fig. 2 yields,

$$\mathfrak{F}(C_0)=\frac{1}{2}S_0(\sigma) \tag{6}$$

$$\mathfrak{F}(C_2)=\frac{1}{4}S_1(\sigma)\exp(-j\phi_2) \tag{7}$$

$$\mathfrak{F}(C_3)=\frac{1}{8}\left(S_2(\sigma)-jS_3(\sigma)\right)\exp(-j\phi_1)\exp(-j\phi_2) \tag{8}$$

Hence, by measuring a known state of polarization (SOP), the modulating phase factors in C_2 and C_3 can be calibrated out and the unknown values reconstructed. This model shows that we can perform reconstructions directly from the interferogram, which is two steps closer to the reconstruction than if we were using a diffraction grating. Here, the interferometer eliminates a wavelength to wave-number interpolation (when using a fast Fourier transform) in addition to an inverse Fourier transform to convert the spectrum from frequency space into the time domain.

3. Reference beam calibration

A method for calibration of the channeled spectropolarimeter is known as the "reference beam calibration technique" [5]. In this form of calibration, the phase factors $\exp(-j\phi_1)$ and $\exp(-j\phi_2)$ found in channels C_2 and C_3 are measured by use of a known input SOP. These "reference data" are then divided by the unknown sample data per Eq. 9 through Eq. 13 below,

$$S_{0,reference}(\sigma)=\left|\mathfrak{F}\left(C_{0,reference,22.5^\circ}\right)\right| \tag{9}$$

$$S_{0,sample}(\sigma)=\left|\mathfrak{F}\left(C_{0,sample}\right)\right| \tag{10}$$

#83298 - $15.00 USD Received 22 May 2007; revised 13 Sep 2007; accepted 14 Sep 2007; published 21 Sep 2007

$$S_{1,sample}(\sigma) = \Im\left[\frac{\mathfrak{F}\left(C_{2,sample}\right)}{\mathfrak{F}\left(C_{2,reference,22.5°}\right)}\frac{S_{0,reference}}{S_{0,sample}}\right] \tag{11}$$

$$S_{2,sample}(\sigma) = \Re\left[\frac{\mathfrak{F}\left(C_{3,sample}\right)}{\mathfrak{F}\left(C_{3,reference,22.5°}\right)}\frac{S_{0,reference}}{S_{0,sample}}\right] \tag{12}$$

$$S_{3,sample}(\sigma) = \Im\left[\frac{\mathfrak{F}\left(C_{3,sample}\right)}{\mathfrak{F}\left(C_{3,reference,22.5°}\right)}\frac{S_{0,reference}}{S_{0,sample}}\right] \tag{13}$$

In most cases, reference data collected with a linear polarizer oriented at 22.5° is sufficient for the reference data set. However, this is not sufficient if dichroism in the retarders is present, as will be described in §6. It should be noted that this method was chosen over the more sophisticated self-calibration technique since our retarders are not setup appropriately (in a compact enclosure and in contact) to make the necessary assumption that both retarders experience identical environmental changes. Additionally, the dichroism in the retarders also complicates the self-calibration technique by modulating S_2 and S_3 directly into one of the channels (for a 2:1 ratio). This is also highlighted in §6.

4. Experimental setup

The FTS equipment that is used for our experiments is an Oriel MIR8000 with an 80026 MCT detector and 80007 Silicon Carbide source. The crystal retarders are made from YVO_4 and are AR coated for 4 μm. The thickness ratio used is 2:1 for d_2:d_1 where d_2 = 4 mm and d_1 = 2 mm. The experimental setup can be seen in Fig. 3; it consists of a wire-grid generating polarizer (G) to allow known SOP input for calibration and sample data measurements. This is followed by the two retarders (R_1 and R_2), wire-grid analyzer (A), and finally the FTS.

The use of the linear polarizer as a target in this instance enables the collection of well-known and stable reference data and input states. However, this generator lacks the ability to produce nonzero S_3. It is already well established that the system configuration can reconstruct this component [2]. Instead, this paper will use the fact that S_3 is zero to examine phase errors due to the interferometer's mechanical instabilities, which is described in §7.

For all of the experiments, data were averaged over 128 consecutive interferograms and obtained for the generating polarizer at orientations ranging from 0° to 180° in 10° increments. Reference data were acquired after each measurement so that thermal effects would not obscure the error analysis. Thermal calibration drift is described in detail in Ref. [5] and correction algorithms exist if certain assumptions about the system setup can be made.

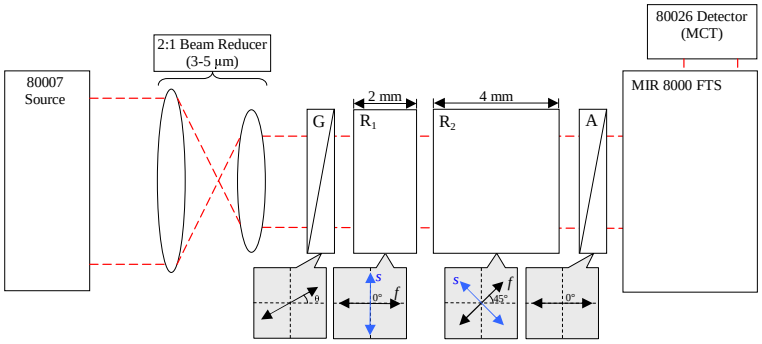

Fig. 3. The experimental setup consists of the MWIR source, generating polarizer G, the two retarders R_1 and R_2, the Analyzer A, and the FTS with the MCT detector.

#83298 - $15.00 USD Received 22 May 2007; revised 13 Sep 2007; accepted 14 Sep 2007; published 21 Sep 2007

5. Experimental results

Using the above model for our reconstructions, we obtained experimental data for the generated state of polarization (SOP) at various rotation angles of the generating polarizer (θ in Fig. 3). In this case, all reconstructions were performed with double-sided interferograms that have been phase-corrected so that they are symmetric using the square-root phase correction technique [6]. The data obtained as a function of polarizer rotation angle and wavelength, portrayed in contour plots, can be seen below in Fig. 4 along with its error in Fig. 5. Here we note that the contours of the data in Fig. 4 should ideally consist of straight lines for S_1 and S_2. Furthermore, if one wavelength is chosen and the Stokes vector visualized as a function of rotation angle, S_1 should appear cosinusoidal and S_2 should appear sinusoidal.

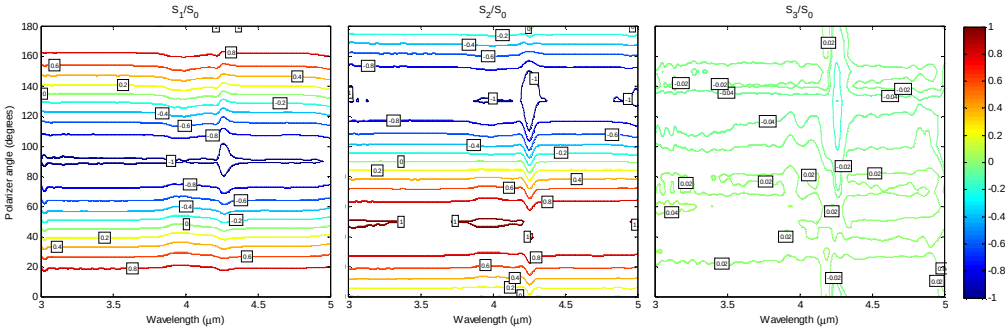

Fig. 4. Contour plots of the initial reconstruction results for the normalized Stokes parameters S_1, S_2, and S_3 using the model per §2 with channels C_0, C_2, and C_3. The spectral resolution is approximately 72 cm^{-1}.

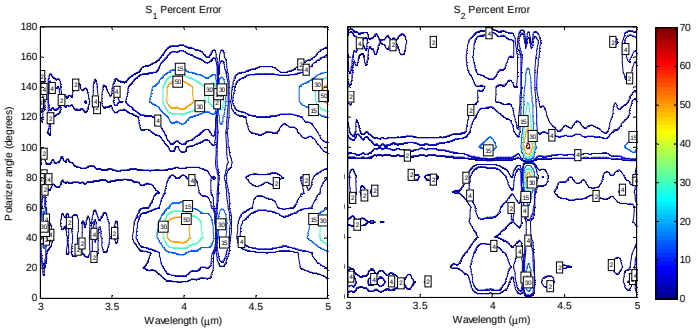

Fig. 5. Contour plots of the percent error in the reconstruction for S_1 and S_2. The relative percent error is undefined for S_2 at 0°, 90°, and 180°. Therefore it has been set to zero for these values.

As can be noted from the reconstruction results, there are several abnormalities in the data. The first corresponds to an expected aliasing anomaly located at 4.28 μm from the sharp CO_2 absorption line, which can always be reduced by nitrogen purging the instrument's air path if required. Other problems with the data occurs around 4 μm and 4.8 μm that are due to absorption features in the YVO_4 crystal (e.g. dichroism) that is not accounted for by the initial model. To see how the error can be explained by the dichroism, a transmission plot for our 2 mm thick YVO_4 retarder for the fast and slow axes, as well as the transmission difference, can be seen in Fig. 6. The error observed in S_1 follows the dichroism very closely, indicating that it is related to the observed phenomena in the reconstructed data.

#83298 - $15.00 USD Received 22 May 2007; revised 13 Sep 2007; accepted 14 Sep 2007; published 21 Sep 2007

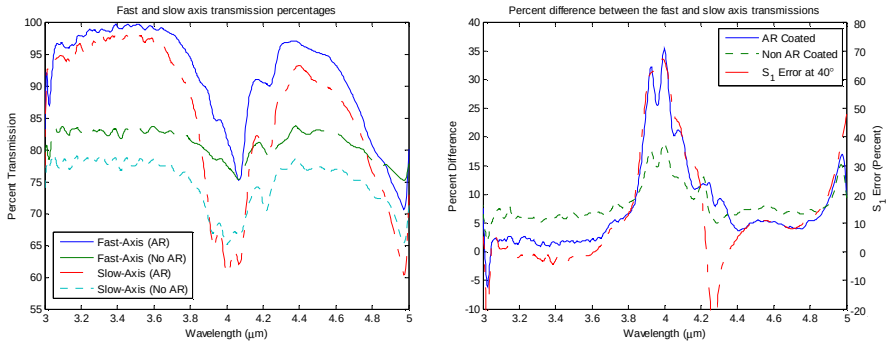

Fig. 6. (Left) Percent transmission of the AR coated 2 mm retarder and a 0.73 mm non-AR coated YVO_4 retarder. The absorption feature is present in both. (Right) Percent difference between the fast and slow axis transmission for the AR coated and non-AR coated samples, as well as a scaled overlay of the S_1 error at 40° to visualize how well its features correspond to the dichroism.

6. Improved model

The model described in §2 works well for crystal materials such as calcite and quartz in the visible spectrum. However, when experiments are carried out in the infrared, dichroism can contribute significant error to the reconstructions. This is an issue since it creates polarization leakage between the Stokes parameters. To investigate this more closely, an improved model was produced by placing theoretical diattenuators behind both retarders per Fig. 7 below.

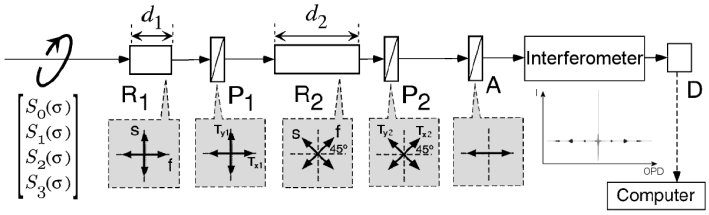

Fig. 7. Improved system model layout. Partial polarizers P_1 and P_2 with transmission attenuation coefficients T_{x1}, T_{x2}, T_{y1}, and T_{y2} have been included to simulate the effects of the varying transmission on the reconstructed results.

It should be noted that the position of the diattenuators in the system, either before or after the retarders, is of no consequence on-axis since the dichroism is aligned to the eigenvectors of the crystal. Using Muller calculus leads us to Eq. 14 below [7].

$$I(\sigma) \propto \frac{(1+\cos(\phi_x))}{2}\left[\begin{array}{l} \frac{S_0}{4}\left(\frac{1}{2}\left(T_{x1}+T_{y1}\right)\left(T_{x2}+T_{y2}\right)+\sqrt{T_{x2}T_{y2}}\left(T_{x1}-T_{y1}\right)\cos(\phi_2)\right)+ \\ \frac{S_1}{4}\left(\frac{1}{2}\left(T_{x1}-T_{y1}\right)\left(T_{x2}+T_{y2}\right)+\sqrt{T_{x2}T_{y2}}\left(T_{x1}+T_{y1}\right)\cos(\phi_2)\right)+ \\ \frac{S_2}{2}\left(\frac{1}{2}\sqrt{T_{x1}T_{y1}}\left(T_{x2}-T_{y2}\right)\cos(\phi_1)+\sqrt{T_{x1}T_{y1}T_{x2}T_{y2}}\sin(\phi_1)\sin(\phi_2)\right)+ \\ \frac{S_3}{2}\left(\frac{1}{2}\sqrt{T_{x1}T_{y1}}\left(T_{x2}-T_{y2}\right)\sin(\phi_1)-\sqrt{T_{x1}T_{y1}T_{x2}T_{y2}}\cos(\phi_1)\sin(\phi_2)\right) \end{array}\right] \quad (14)$$

Analysis of this equation yields three key results:

#83298 - $15.00 USD Received 22 May 2007; revised 13 Sep 2007; accepted 14 Sep 2007; published 21 Sep 2007

1. The S_0 and S_1 components are mixing between each other in spectral locations where there are differences between T_{x1} and T_{y1}, as can be seen from the difference terms in the first and second lines.
2. Portions of S_2 and S_3 are directly modulated by φ_1, and consequently their energy appears as an additional modulation in the C_1 channel (see Fig. 3). This complicates the channel's ability to reconstruct data accurately. Here we note that in a 1:3 ratio design (d_2:d_1), *these data would appear in an empty channel*, meaning all channels still remain usable. It would also preserve the self-calibration technique outlined by Oka without requiring further calibration steps.
3. S_2 and S_3 can be reconstructed and calibrated in the traditional sense if one uses channel C_3 or its conjugate (e.g. $(\varphi_1 + \varphi_2)$ or $-(\varphi_1 + \varphi_2)$). However, error will still be present in the reconstruction of these channels due to the normalization of S_2 and S_3 to S_0. This is due to mixing between S_1 and S_0 when S_1 is nonzero.

Therefore it can be presumed that error due to the dichroism can be compensated for if one knows T_{x1}, T_{y1}, T_{x2}, and T_{y2}, information which can be extracted from the data in Fig. 6.

6.1 Improved calibration procedure

The modified calibration procedure that will be described here requires measuring the transmission of the fast and slow axes of the first retarder (R_1), in addition to collecting reference data with a linear polarizer at 0° and 45°. If we start by taking the sample data for S_0 and S_1, along with the reference spectra taken at 0°, we have,

$$S_{0,sample}(\sigma) = \left|\mathfrak{F}\left(C_{0,sample}\right)\right| = \left(S_0\gamma + S_1\varepsilon\right) \tag{15}$$

$$S_{1,sample}(\sigma) = \Re\left[\frac{\mathfrak{F}\left(C_{2,sample}\right)}{\mathfrak{F}\left(C_{2,reference,0^\circ}\right)}\frac{\left|\mathfrak{F}\left(C_{0,reference,0^\circ}\right)\right|}{\left|\mathfrak{F}\left(C_{0,sample}\right)\right|}\right] = \frac{S_0\varepsilon + S_1\gamma}{S_0\gamma + S_1\varepsilon} \tag{16}$$

Here, Eq. (14) has allowed us to write out the analytical form of the calibrated channels with the absorption terms, where $\gamma = T_{x1} + T_{y1}$ and $\varepsilon = T_{x1} - T_{y1}$. We now wish to extract the original input, S_1 and S_0. Solving for these terms yields,

$$S_0 = S_{0,sample}\frac{\varepsilon S_{1,sample} - \gamma}{\left(\varepsilon^2 - \gamma^2\right)} \tag{17}$$

$$S_1 = S_{0,sample}\frac{\varepsilon - \gamma S_{1,sample}}{\left(\varepsilon^2 - \gamma^2\right)} \tag{18}$$

Note that the above S_1 is un-normalized. The final normalized output is then,

$$S_{1,corrected} = \frac{S_1}{S_0} \tag{19}$$

We now have a corrected measurement for S_1. Since S_2 and S_3 don't suffer additional error from the dichroism (as long as channel C_3 is used for reconstruction in a 2:1 ratio system) except from the normalization to S_0, we only need to correct the S_0 that's seen in the S_2 and S_3 reference data. This is where the 45° reference data is used since S_1 is zero for this input, meaning that the S_0 component has the form,

#83298 - $15.00 USD Received 22 May 2007; revised 13 Sep 2007; accepted 14 Sep 2007; published 21 Sep 2007

$$S_{0,reference}(\sigma) = \left|\mathfrak{F}\left(C_{0,reference,45^\circ}\right)\right| = S_0'\gamma \tag{20}$$

where the prime is used to indicate that this is not the same S_0 as in Eq. (17). Now, we only have to divide by γ to correct S_2 and S_3,

$$S_{2,corrected} = \Re\left[\frac{\mathfrak{F}\left(C_{3,sample}\right)}{\mathfrak{F}\left(C_{3,reference,45^\circ}\right)}\frac{S_{0,reference}(\sigma)}{S_0(\sigma)}\right]\frac{1}{\gamma} \tag{21}$$

$$S_{3,corrected} = \Im\left[\frac{\mathfrak{F}\left(C_{3,sample}\right)}{\mathfrak{F}\left(C_{3,reference,45^\circ}\right)}\frac{S_{0,reference}(\sigma)}{S_0(\sigma)}\right]\frac{1}{\gamma} \tag{22}$$

Hence the Stokes vectors S_1, S_2, and S_3 can have the dichroic contribution from the retarders fully corrected with this method.

7. Interferometer instability

An explanation as to why data are present in the S_3 reconstruction, peaking on the order of 4% when it should be closer to zero, is likely due to mechanical instabilities in the interferometer. Here, two forms of interferometer instability will be analyzed, namely displacement of the center-burst from zero OPD and unevenly spaced sampling of the interferogram.

7.1 Displaced center-burst

If the center burst location of the interferogram differs *between* the reference and sample data by some OPD Δz, then the reconstructed spectra will suffer a phase change of $\Delta\phi = 2\pi\Delta z/\lambda$. This term will appear in the Fourier transform as an additional exponential phase factor, which will cause the real and imaginary components of the reconstruction to alias. Our reference and sample data Fourier transforms become

$$\mathfrak{F}\left(C_{2,reference}\right) = \frac{1}{4}S_1(\sigma)\exp\left(-j\phi_2(\sigma)\right) \tag{23}$$

$$\mathfrak{F}\left(C_{3,reference}\right) = \frac{1}{8}\left(S_2(\sigma) - jS_3(\sigma)\right)\exp\left(-j\phi_1(\sigma)\right)\exp\left(-j\phi_2(\sigma)\right) \tag{24}$$

$$\mathfrak{F}\left(C_{2,sample}\right) = \frac{1}{4}S_1(\sigma)\exp\left(-j\phi_2(\sigma)\right)\exp\left(j\Delta\phi\right) \tag{25}$$

$$\mathfrak{F}\left(C_{3,sample}\right) = \frac{1}{8}\left(S_2(\sigma) - jS_3(\sigma)\right)\exp\left(-j\phi_1(\sigma)\right)\exp\left(-j\phi_2(\sigma)\right)\exp\left(j\Delta\phi\right) \tag{26}$$

Division between the sample and reference data of channels C_2 and C_3 while taking the real and imaginary parts where appropriate yields

$$\Re\left[\mathfrak{F}\left(C_{2,sample}\right) \Big/ \mathfrak{F}\left(C_{2,reference}\right)\right] = S_1(\sigma)\cos(\Delta\phi) \tag{27}$$

$$\Re\left[\mathfrak{F}\left(C_{3,sample}\right) \Big/ \mathfrak{F}\left(C_{3,reference}\right)\right] = S_2(\sigma)\cos(\Delta\phi) \tag{28}$$

$$\Im\left[\mathfrak{F}\left(C_{3,sample}\right) \Big/ \mathfrak{F}\left(C_{3,reference}\right)\right] = S_3(\sigma)\sin(\Delta\phi) \tag{29}$$

Hence, the Stokes components S_1, S_2, and S_3 are multiplied by a sinusoidal error term proportional to the phase offset between the reference and sample data. Fortunately, this issue

#83298 - $15.00 USD Received 22 May 2007; revised 13 Sep 2007; accepted 14 Sep 2007; published 21 Sep 2007

can be resolved relatively well by phase-correcting the interferogram (for double-sided interferograms) in the following way,

$$W'(\sigma) = \Im\left[I(\sigma, z)\right] = W_R(\sigma) + jW_I(\sigma) \tag{30}$$

$$W(\sigma) = \left|W'(\sigma)\right| = \left(W_R^2(\sigma) + W_I^2(\sigma)\right)^{1/2} \tag{31}$$

This is the square-root method alluded to earlier. Here $W_R(\sigma)$ and $W_I(\sigma)$ are the real and imaginary parts of the interferogram's Fourier transform, respectively. Taking the absolute value of the spectrum will yield the magnitude spectrum $|W(\sigma)|$, which contains no phase errors sans small noise non-linearity's [1]. The symmetric interferogram, $I'(z)$, can then be obtained by an inverse Fourier transform of the magnitude spectrum,

$$I'(z) = \Im^{-1}\left[W(\sigma)\right] \tag{32}$$

We now have a phase-corrected interferogram that is real and symmetric. This process will remove any phase errors associated with a displaced center-burst assuming the center burst begins close to zero OPD [8]. It also provides an additional benefit in that phase discrepancies between the reference and sample data caused by the temporal drift of the interferometer (usually thermal effects) are also corrected.

7.2 Uneven interferogram sampling

It is known that rapid-scan interferometers, such as the one used for our experiments, can have significant errors introduced into spectra from uneven sampling of the interferogram [9]. This is caused by velocity jitter over the course of a scan; it typically contains both random and periodic components. Since the channeled spectropolarimetric technique is sensitive to sub-pixel misregistration between the sample and reference data, it can be a significant problem when trying to perform accurate reconstructions. Here, the misregistration occurs due to the primary assumption in the Fast Fourier Transform (FFT) algorithm: that all data are sampled uniformly.

If we configure the FFT algorithm with an arbitrary sampling function $s(z)$, where z is in units of OPD, we have,

$$U(k) = \sum_{b=-N/2}^{N/2-1} I\left(b \cdot s(z)\right) \exp\left(\frac{j2\pi bk}{N}\right) \tag{33}$$

where N is the total number of samples, I is the interferogram, and U is the FFT of I. If $s(z)$ is a constant, we have the ideal sampling situation (e.g. $s(z)$ = 316.4 nm, the nominal value in our interferometer). However, if $s(z)$ varies linearly, randomly, or otherwise, error can be introduced into the reconstructed spectrum. Such error usually manifests itself as a form of aliasing and affects data at higher frequencies more than lower [10]. For instance, real spectral data from our FTS using two consecutive measurements yields the two magnitude spectra in Fig. 8.

As can be seen, the modulations in the dashed line are severely attenuated and distorted compared to the solid line. It must be emphasized here that such low-visibility spectral measurements from our instrument are rare; however they can occur during the course of data averaging hundreds of interferograms.

#83298 - $15.00 USD Received 22 May 2007; revised 13 Sep 2007; accepted 14 Sep 2007; published 21 Sep 2007

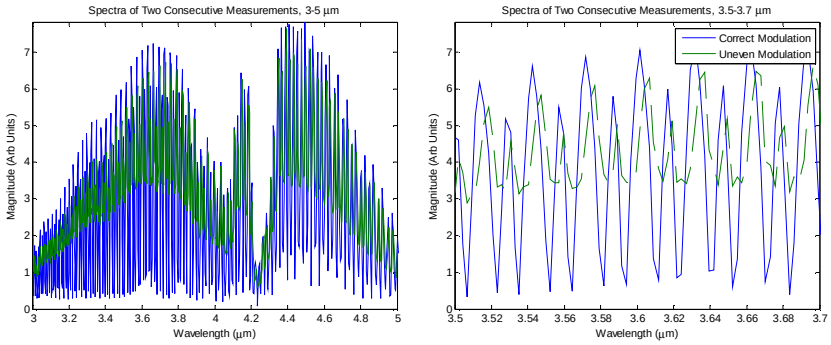

Fig. 8. Two consecutive spectral measurements taken with our FTS of a linear polarizer at 22.5°. The solid (blue) line indicates a relatively evenly sampled interferogram, whereas the dashed (green) line is indicative of uneven sampling occurring.

7.3 Correction of nonuniformally sampled interferograms

Although it can not be tested experimentally with our current interferometer, it is envisioned that the best way to correct the remaining error due to nonuniform sampling in the data is to use a Nonuniform Fast Fourier Transform (NuFFT) or a spline-interpolation algorithm [11,12]. Unfortunately, this requires *a priori* knowledge of how the interferogram has been sampled in order for the algorithm to convert it to a uniformly sampled dataset. But we can investigate the algorithm's effectiveness of correcting a channeled interferogram's nonuniform sampling in simulation. Here, we chose to investigate the NuFFT algorithm. Using an arbitrary sampling function defined as

$$bs(z) = 316.4\times10^{-9}\left[b - 10\left(1-\frac{4b^2}{N^2}\right)\right], \quad -\frac{N}{2} \le b \le \frac{N}{2}-1 \tag{34}$$

and defining the error as the difference between the ideal sampling, $bs(z) = 316.4\times10^{-9}b$ and Eq. (34) gives,

$$\varepsilon = 316.4\times10^{-9}\left[10\left(1-\frac{4b^2}{N^2}\right)\right], \quad -\frac{N}{2} \le b \le \frac{N}{2}-1 \tag{35}$$

This yields the quadratic sampling error versus sample index (b) seen in Fig. 9. Here it can be seen that the error is large with a peak of 3.16 μm (10 pixels) at the center of the interferogram.

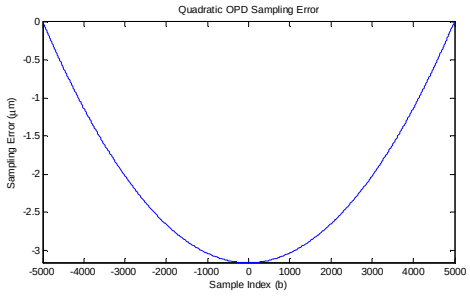

Fig. 9. Quadratic sampling error used for the simulated nonuniformally sampled interferogram.

#83298 - $15.00 USD Received 22 May 2007; revised 13 Sep 2007; accepted 14 Sep 2007; published 21 Sep 2007

Simulating the interferometer with the same input spectrum as our experimental setup yields the following output results per Fig. 10.

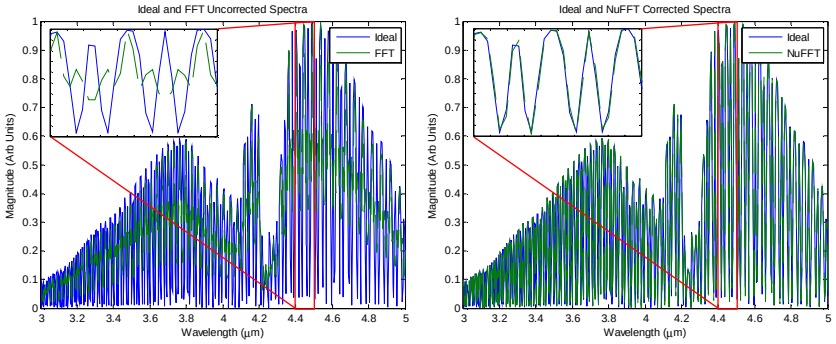

Fig. 10. Ideal channeled spectra and the spectra reconstructed after nonuniform sampling with (left) the normal FFT (which assumes uniform spacing) and (right) the NuFFT (setup with an over-sampling factor of m = 2 and q = 8).

The spectral reconstruction done with the NuFFT is superior to that of the FFT. Comparison between the NuFFT and the ideal spectra in a Stokes vector reconstruction yields a maximum error of approximately 1.6% in S_1 from channel C_2, 0.4% in S_{23} from channel C_1 and 3.6% in S_{23} from channel C_3. This confirms that the higher frequency data, as is seen in the outermost channel, is affected the most by the nonuniform sampling. It also emphasizes the algorithm's ability to compensate for the nonuniform sampling given a channeled spectrum.

7.4 Further phase calibration

All of the aforementioned issues play a roll in the errors contributed to the reconstruction. These phenomena typically manifest themselves as errors in the phase between the reference and sample data consisting of a small linear term plus some constant offset. To illustrate this effect, the residual phase from the 0° S_1 reconstruction (before taking the real part of the Fourier transform) is shown in Fig. 11.

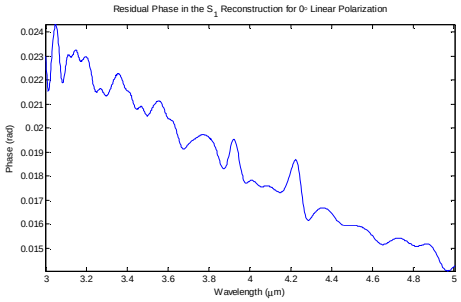

Fig. 11. Residual phase in the S_1 reconstruction. It consists of a linear term in addition to a constant offset.

Such error causes some of the information about the Stokes vectors to be lost (in the case of S_1) or aliased (in the case of S_2 and S_3) when the real or imaginary parts are extracted.

In order to alleviate the residual phase error, it was initially assumed that the function in Fig. 11 could be approximated by a static translation in phase between the reference and sample channels. Additionally, we are making the assumption that the temperature change of

#83298 - $15.00 USD Received 22 May 2007; revised 13 Sep 2007; accepted 14 Sep 2007; published 21 Sep 2007

the retarders is negligible between sample and reference data, such that most of the phase error is due to the mechanical instabilities of the instrument. The static phase error can be modeled using the formulas of §6.1. The goal is to approximate this phase difference ($\Delta\varphi$) using only the reference and sample data provided. Beginning by dividing Eq. (25) by (23) and (26) by (24) yields,

$$\Big/ \Im\left(C_{2,reference,0^\circ}\right) = S_1(\sigma)\exp\left(j\Delta\phi_{0^\circ}\right) \tag{36}$$

$$\Big/ \Im\left(C_{3,reference,45^\circ}\right) = \left(S_2(\sigma) - jS_3(\sigma)\right)e^{j\Delta\phi_{45^\circ}} = \left|S_{23}(\sigma)\right|\exp\left(-j\phi_{23}\right)\exp\left(j\Delta\phi_{45^\circ}\right) \tag{37}$$

where the additional subscripts, 0° and 45°, indicate which set of reference data are being used (e.g. the reference linear polarizer's orientation). Hence, any phase error that exists between the reference and sample data is isolated in the C_2 channel for the S_1 reconstruction, while it is combined with the S_{23} phase in the C_3 channel for the S_2 and S_3 reconstructions. Therefore, any imaginary part in the S_1 reconstruction can be attributed to an error resulting from a misregistration between the reference and sample data. This phase difference can be approximated as long as there is enough signal in the S_1 state during the measurement.

Fortunately, this is always true due to the dichroism of the YVO_4 retarders. From Eq. (14), we see that the dichroic contribution from S_0 to S_1 is largest where $\left(T_{x1} - T_{y1}\right)$ is largest. This occurs from 3.9-4.1 μm (2577-2419 cm^{-1}) (see Fig. 6, right). As a result, the phase offset can be approximated by averaging the phase difference in this spectral region over wavelength and the conjugate of this phase can be applied to the entire spectrum to correct it. This dichroic contribution is extremely important for the 45° S_{23} reference data, considering no signal in the S_1 channel is ideally present in the absence of the dichroism.

In the following equations, the < > operation indicates that the arithmetic mean has been taken and the subscripts *R* and *I* refer to the real and imaginary parts of the output, respectively. We first obtain for the S_1 reconstruction,

$$S_1'(\sigma) = \Im\left(C_{2,sample}\right) \Big/ \Im\left(C_{2,reference,0^\circ}\right) = S_{1,R,0^\circ}(\sigma) + jS_{1,I,0^\circ}(\sigma) \tag{38}$$

$$\phi_0' \simeq \left\langle \operatorname{atan}\left(S_{1,I,0^\circ}(\sigma) \Big/ S_{1,R,0^\circ}(\sigma) \right) \right\rangle, \quad \left(2419 \le \sigma \le 2577\ \mathrm{cm}^{-1}\right) \tag{39}$$

$$S_1(\sigma) = S_1'(\sigma)\exp\left(-j\phi_0'\right) \tag{40}$$

Similarly, for S_{23},

$$S_1'(\sigma) = \Im\left(C_{2,sample}\right) \Big/ \Im\left(C_{2,reference,45^\circ}\right) = S_{1,R,45^\circ}(\sigma) + jS_{1,I,45^\circ}(\sigma) \tag{41}$$

$$S_{23}'(\sigma) = \Im\left(C_{3,sample}\right) \Big/ \Im\left(C_{3,reference,45^\circ}\right) \tag{42}$$

$$\phi_{45}' = \left\langle \operatorname{atan}\left(S_{1,I,45^\circ}(\sigma) \Big/ S_{1,R,45^\circ}(\sigma) \right) \right\rangle, \quad \left(2419 \le \sigma \le 2577\ \mathrm{cm}^{-1}\right) \tag{43}$$

$$S_{23}(\sigma) = S_{23}'(\sigma)\exp\left(-j\phi_{45}'\right) \tag{44}$$

This method works in general in the laboratory, although care in selecting the lower limit on σ in Eq. (39) and (43) must be taken to avoid the CO_2 absorption line for larger air paths (ours is

#83298 - $15.00 USD Received 22 May 2007; revised 13 Sep 2007; accepted 14 Sep 2007; published 21 Sep 2007

~1 m). This is important since the peak dichroic region of the YVO_4 is close to the CO_2 absorption band.

8. Results with improved calibration

Using the improved model to calibrate the system reveals a marked improvement in the reconstruction. The new reconstruction can be seen in Fig. 12 along with its error in Fig. 13.

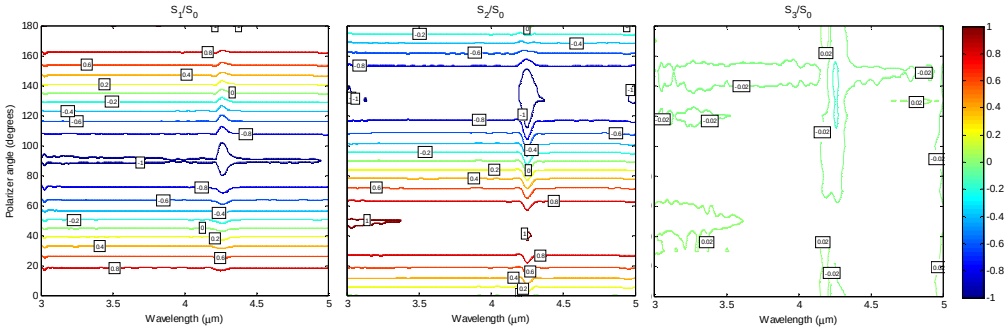

Fig. 12. Contour plots of the reconstruction results for the normalized Stokes parameters S_1, S_2, and S_3 using the improved model per. §6 and §7.4. The spectral resolution is approximately 72 cm^{-1}.

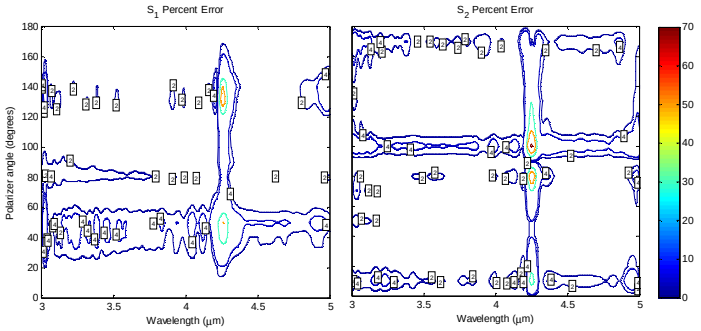

Fig. 13. Contour plots of the percent error in the improved reconstructions. Large error is still present near the CO_2 absorption line.

The abnormalities in the data around 4 μm and 4.8 μm are significantly diminished, reducing the error around the crystal's dichroic regions by nearly 20 times. Additionally, the S_3 reconstruction is improved by use of the modified calibration (§7.4). For these measurements, positioning error of the generating polarizer (+/- 0.10°) is expected to account for negligible error (< 0.01%) when S_1 or S_2 are at their maxima and 2% when at their minima.

9. Conclusion

From the above analysis and experimentation in the laboratory, it is apparent that there are several issues when operating a channeled spectropolarimeter in the infrared which contribute to an increase in error. These include:

1. Aliasing effects. These will always limit the maximum achievable accuracy of this technique. This was seen to some extent in the CO_2 absorption line and can be a significant issue if *a priori* knowledge of aliasing effects cannot be obtained (e.g. via subtraction of an unpolarized reference spectrum).

#83298 - $15.00 USD Received 22 May 2007; revised 13 Sep 2007; accepted 14 Sep 2007; published 21 Sep 2007

2. Dichroism in the retarders. This phenomenon can create significant error; however the improved calibration technique can be utilized to compensate for its effect on the reconstructions.

Other issues directly related to the use of an interferometer highlight the importance of taking into consideration issues with the mechanical instabilities of the system. Primarily, these can be addressed by double-sided interferogram phase correction (by using the magnitude spectrum) and compensating in some way for the nonuniform sampling (through interpolation or the NuFFT).

Ultimately the average absolute system error outside of the CO_2 absorption line, focusing on the regions with the largest dichroism (4.4-5.0 μm and 3.7-4.1 μm) over all the measurements was brought down from 8.72% for S_1 and 2.84% for S_2 to 1.07% for S_1 and 1.06% for S_2. Additionally, the average absolute error of S_3 was brought down from 2.2% to 1.06%. Since our generating polarizer has an extinction ratio of around 100:1, this is essentially the limit of our equipment. This demonstrates that the Fourier transform spectropolarimetric technique shows significant promise in the infrared wavelengths for performing spectropolarimetric measurements.

Further improvements to the system that can be accomplished include moving to a 1:3 ratio between the retarder thicknesses such that all channels can be used in the reconstruction. Another improvement would be to mount the retarders close together in a small enclosure. These two changes would then enable the use of the self-calibration technique (or a modified version thereof that takes into account the dichroism), which would make the system calibration relatively insensitive to temperature changes in the retarders.

#83298 - $15.00 USD Received 22 May 2007; revised 13 Sep 2007; accepted 14 Sep 2007; published 21 Sep 2007